

A Fully Automated Image Analysis Framework for Quantitative Assessment of Temporal Tumor Changes

Georgios C. Manikis¹, Dimitra Emmanouilidou¹, Vangelis Sakkalis¹, Norbert Graf², Kostas Marias¹

¹ Computational Medicine Laboratory, Institute of Computer Science, Foundation for Research and Technology, Hellas

² University Hospital of the Saarland, Homburg, Germany

gmanikis@ics.forth.gr, dimitra.emmanouilidou@gmail.com, sakkalis@ics.forth.gr, norbert.graf@uniklinikum-saarland.de, kmarias@ics.forth.gr

Abstract- This paper presents a novel framework for assessing tumor changes based on histogram analysis of temporal Magnetic Resonance Image (MRI) data. The proposed method detects the distribution of tumor and quantitatively models its growth or shrinkage offering the potential to assist clinicians in objectively assessing subtle changes during therapy. The presented work and the initial validation refer to the glioma case but can be generalized to any type of cancer where medical imaging is routinely used to characterize tumor response over time.

Keywords- *cancer image analysis; MRI; glioma; histogram analysis; quantitative imaging*

I. INTRODUCTION

Gliomas are the most common brain tumors. The incidence of gliomas in the United States and in Europe is about 7-11/100.000 of the population and significantly higher than in Asia with 2-4/100.000 [1]. Among gliomas about 50% are high grade glioblastoma (grade III) according to WHO classification system [2], but strikingly even a histologically relatively well-differentiated glioma can become biologically highly malignant. In addition, gliomas show the inherent capacity to progress to a more malignant phenotype.

For the diagnosis of a patient experiencing the signs and symptoms of a brain tumor, neuroradiologic imaging is the main diagnostic modality used. Magnetic resonance imaging (MRI) has become the method of choice. Usually gadolinium-enhanced (Gd) MRI confirms the diagnosis of a brain tumor, and may also indicate a specific tumor type, where the initial surgical resection is the treatment of choice. Due to the high rate of recurrence in malignant gliomas the adjuvant radiation therapy is indispensable at least in malignant gliomas as part of the standard-of-care therapy.

To assist the crucial work of the clinician, automated (or semi-automated) tools can provide objective, reproducible and in many cases quantitative information for improving diagnosis and prognosis accuracy. In this context, tools for evaluating tumor expansion or shrinkage are critical for supporting individualization of cancer treatment. The aim of the current work is to assess and follow-up the brain tumor

progression of a patient, using all his/her available examinations during the whole therapeutic treatment and quantify the individual course of treatment. Changes on intensity distributions of tumoral areas can provide valuable information and knowledge on patient's treatment response.

I. ASSESSMENT OF RESPONSE AND PROGRESSION

In 1990, the MacDonald Criteria [3] for response assessment in high-malignant gliomas were introduced, and in 2000 the Response Evaluation Criteria in Solid Tumors (RECIST) were presented and were recently revised in [6]. Still there have been no studies prospectively validating the RECIST criteria in gliomas. Therefore the MacDonald Criteria are still widely used as a reference for assessing tumor response in clinical trials, but are subject to a number of significant limitations [7].

Manual delineations of suspicious brain lesions is routinely used as the gold standard but it is time consuming, observer-dependent and in some difficult cases prone to error (e.g. distributed timorous areas with low image contrast). As a result, temporal cancer tissue changes are difficult to assess with manual delineations, stressing the need for objective measures for quantifying changes. To address the above needs, several automated and semi-automated techniques for tumor identification exist in the literature. In [8], a thorough review of widely used techniques for detection and diagnosis of disease was presented. Recent studies [9]-[11] proposed a medical image analysis system to segment and follow-up brain tumors, using integrated information from multiple MRI modalities. Relevant features are extracted from the 3D volume, consisting of signal intensities, texture values and transformation coefficients. Finally, a diagnostic framework is applied to the meta-dataset, derived from these features.

Image segmentation is a prerequisite step in all frameworks mentioned above. A wide variety of approaches have been proposed for image segmentation either based on the spatial properties of the image such as edges and regions [12]-[14] or on more sophisticated statistical pattern recognition techniques [15]-[22]. Most of these studies combine multiple MRI

modalities to segment tumor volumes, in a way of extracting complementary information to resolve some ambiguities.

A fast and accurate registration is a preliminary step when tumor regions are segmented from multiple MRI. However, being an area-based technique, multimodal registrations have principal limitations to robustness and reliability. To overcome these problems iterative and backtracking techniques are adopted, but they often increase the computational complexity [23]. In the frame of medical imaging, skull stripping is also prerequisite step towards a better segmentation. More accurate results are generated when the brain tissue is isolated from the skull and non-brain intracranial tissues. However, skull striping techniques are often susceptible to problems due to the large anatomical variability of the brain and require manual intervention [24]. Segmentation algorithms may also introduce errors due to the deformation near the structures in the brain, the variety of shapes and the lack of a priori knowledge about the tumor volume. Furthermore, several segmentation techniques are time expensive and increase the overall framework's executing time.

In recent clinical work [25], it was shown that histograms of signal intensities between cerebrospinal fluid (CSF), vital tumor, necrotic and cystic areas within the tumor vary consistently with patient response to therapy in all modalities analyzed. Using this imaging biomarker information, it might become possible to describe quantitative histogram biomarker changes in the tumor during the follow-up of single patients that are correlated to treatment response or progression. The results of this study indicated that the higher the standardized median and mean values of signal intensities in T1 during the follow-up of a single patient, the more likely the patient suffers from progression of disease. If these values are reducing it is more likely that a tumor response can be established, as shown in Figure 1.

These observations led us to the hypothesis that temporal histogram analysis framework can potentially provide objective differential information concerning brain tissues by

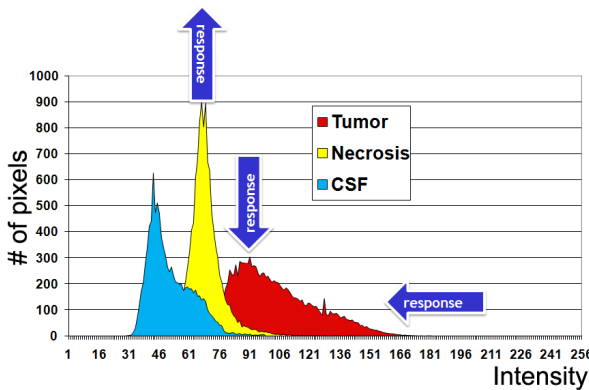


Figure 1. Histogram changes with regard to treatment response, as observed by clinicians. Response is usually accompanied by high-peak necrotic area and low-peak tumor area distributions with low variance.

using the characteristics of its distributions. Based on this, the proposed framework, depicted in Figure 2, would require no registration, segmentation and skull striping. The proposed differential histogram analysis framework takes no account of the spatial registration of 3D volumes and may avoid/surpass such constraints focusing only in the processing of the signal intensities of the 3D MRI volume.

II. MATERIALS AND METHODS

Due to the highly invasive nature of glioma in the vast majority of cases patient are operated after diagnosis. For this reason, it is rarely the case that temporal cancer data before and after therapy is available. From a pool of brain glioma datasets three patient datasets P1, P2 and P3 were used. The data was acquired by different sequence modalities on distinct follow-up times as shown in TABLE I. . For subjects P2 and P3 the time presented under study date field denote the acquisition time after surgery. Examinations were acquired on a 1.49 Tesla MR Siemens scanner with 5mm slice thickness Areas of CSF, Cyst, Tumor, Necrosis and Edema were identified and annotated by a radiologist to use for validation purposes. Though, it is a difficult and enigmatic task for clinicians to define the exact margins of bulk tumor; the exact lesion boundaries are not easily discernible and within each boundary different pathological information may be included. Among available brain volumes, no significant overlap can be found between Tumor and Cyst histograms; a fact that enforces histogram discrimination of malignant areas.

A. Data Preparation

1) Intensity Normalization

Although volume change assessment is restricted to data obtained by the same MR modality and predefined parameters, intensity homogeneity of sequential 3D volumes cannot be guaranteed due to non-linearity involved in the acquisition process. Consequently, prior to our differential histogram analysis the volumes were normalized as proposed in [26], according to

$$h_{xy} = \frac{I_{\max} - I_{\min}}{f_{\max} - f_{\min}} (f_{xy} - f_{\min}) + I_{\min}, \quad (1)$$

where f is the image to be normalized and h is the outputted image. f_{xy} and h_{xy} denote the intensity value at indices (x,y) , and f_{\min} and f_{\max} are the minimum and maximum intensity values, respectively, appeared in f . I_{\min} and I_{\max} denote the minimum and maximum intensity value limits for the outputted image h and were obtained considering all available follow-up examinations.

TABLE I.
SETS USED IN CURRENT STUDY.

Subject	P1	P2	P3
Modality	Gd-enhanced T1	T1 & T2-FLAIR	Gd-enhanced T1
StudyDate	1) On Diagnosis, Before Surgery	1) 3½ months 2) 5 months 3) 8 months	1) 4½ months 2) 7½ months 3) 8½ months

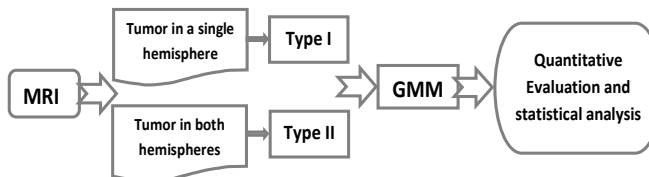


Figure 2. The proposed framework for cancer change assessment.

B. Statistical Method

Gaussian Mixture Modeling (GMM) was applied for curve fitting on histogram distributions. A set of mixed distributions can be accurately distinguished by applying individual Gaussian distributions to the observed data. Competing peaks of tumor with edema and/or cyst led to a choice of two-components for the GMM model:

$$p(\mathbf{x}) = \sum_{i=1}^M w_i g(\mathbf{x} | \boldsymbol{\mu}_i, \Sigma_i) \quad (2)$$

where M is the number of mixture components, in our case $M=2$, \mathbf{x} is the continuous valued vector, w_i are the mixture weights, and $g(\mathbf{x} | \boldsymbol{\mu}_i, \Sigma_i)$ are the component densities. Each component is a Gaussian function of the form

$$g(\mathbf{x} | \boldsymbol{\mu}_i, \Sigma_i) = \frac{1}{\sqrt{2\pi} |\Sigma_i|^{1/2}} \exp\left\{-\frac{1}{2} (\mathbf{x} - \boldsymbol{\mu}_i)^T \Sigma_i^{-1} (\mathbf{x} - \boldsymbol{\mu}_i)\right\}$$

with mean vector $\boldsymbol{\mu}_i$ and covariance matrix Σ_i . The mixtures weight satisfy that $\sum_{i=1}^M w_i = 1$. The complete Gaussian mixture model is parameterized by the mean vectors, covariance matrices and mixture weights from all components densities. Maximization algorithm (EM) was used to estimate the component parameters of the mixture model distribution.

The two components of the outputted model were used to determine intensity boundaries and separate the tumoral histogram distribution from other malignant area distribution. Histogram based features of each component were then extracted and evaluated as discussed in section III.

C. Malignant Tissue Identification

The aim is to identify, localize and quantify any malignant areas present in a 3D MRI. In subjects P1 and P2 such areas were present in only one of the two brain hemispheres, and thus identification Type I was performed, whereas in subject P3, malignant tissue clearly occupied regions of both hemispheres, yielding a different approach, the one proposed in Identification Type II.

1) Identification Type I

As a first step, the 3D volume of the brain hemisphere containing no malignant tissue was marked as BaselineArea (BA), whereas the 3D volume of the brain hemisphere containing malignant tissue was marked as CriticalArea (CA). Since the acquisition modalities used can ensure that malignant areas appear in high intensities, the two hemispheres can easily be distinguished to BA and CA only considering the intensity distributions. The separation of the two hemispheres was manually performed in the current study,

but an automatic segmentation technique can easily be adopted as a preprocessing step, such as the freely available segmentation algorithms on BrainVisa [27] and SurfRelax [29] or using a Graph Cuts segmentation algorithm as in [28]. After histograms BA and CA were obtained, they were subtracted to form the StudyArea (SA) histogram, as in

$$SA(i) = \max\{CA(i) - BA(i), 0\}. \quad (3)$$

The SA distribution reveals the intensity distribution of malignant areas. In case of complete absence of malignant tissue in the brain, the left and right hemispheres are similarly and equally depicted in the histogram; a subtraction of the two hemisphere histograms would result in a negligible spectrum. However, when one of two hemispheres actually contains malignant tissue, the histogram distributions of the hemispheres differ significantly and their simple difference can identify the intensity range and distribution of malignant areas.

The two-component GMM curve fitting was applied on SA histograms of each case study for every subject, identifying the tumoral as well as other malignant regions. The SA histogram may contain considerable low-intensity volume corresponding to background noise, as well as high-intensity volume corresponding to skull areas. Although no sophisticated skull-stripping algorithm was applied as a pre-processing step, rejecting these volumes from the SA histogram is a very simple task. Thus, histogram data underneath the left tail (25th percentile) of the first Gaussian and the right tail (75th percentile) of the second Gaussian were discarded considered outliers.

For cases where malignant areas cover regions of both hemispheres, as is the case for patient P3 or in cases where spatial information of the malignant areas is not available before the identification step, the following framework is proposed, where a different definition of BA and CA areas is considered:

2) Identification Type II

In case where malignant areas exist in both hemispheres, further patient's examinations were used; all 3D image volumes were normalized according to (1). The brain volume of the first (in time) MR examination was marked as BA and constituted the reference examination. Then, each one of the follow-up examination volumes was marked as CA and histograms of BA and CA were subtracted to form the SA distribution, according to (3). GMM curve fitting is then applied on the SA histograms, as described in section III B, using two Gaussian curves and rejecting the low and high intensity values.

Using one of the schemes above, the identification of tumoral and other malignant areas is achieved. Quantification measures for the SA distributions may be used to assess the presence and significance of malignant area and decide if further alert is needed. Volume change assessment of tumoral areas is the next crucial step, especially for follow-up treatment.

D. Tumor Volume Change Assessment

The main goal is to identify and quantify the tumoral area change in the brain. Using the two-component GMM model, two intensity regions were identified on every SA histogram. The region covering the highest intensity values was isolated to simulate tumor's progress and histogram based criteria of this region were extracted for comparison. In addition, histogram specific metrics were calculated for assessing histogram distribution changes during follow-up and all finding are described in the following section.

III. RESULTS

Malignant identification was applied to different acquisition schemes, and the proposed framework was able to discriminate tumoral from other malignant areas. Representative results of malignant identification type I on T1 Gd-enhanced and T1 data are shown in Figure 3 (a-c). In the top subplot of each study case, the identified SA histograms are shown in gray area and two distinct intensity areas are clearly depicted. The clinical expert's annotations are also shown in the plots for evaluation purpose. Results of the two-component Gaussian curve fitting as applied on SA histogram distribution are shown in the bottom subplot of each study case. PDF 1 curve marks the histogram intensity ranges containing tumoral data, whereas PDF 2 curve identifies the intensity ranges of other malignant areas present in the brain volume. Notice in subfigure (a) that PDF 2 covers the necrotic intensity area, in (b) it covers the cystic area and in (c) the edema area. The proposed framework was also tested on T2-FLAIR examination data and the GMM curve fitting model was able to successfully discriminate tumoral from other malignant intensity areas, in Figure 3 (d).

The tumor volume change assessment methodology was applied to subjects P2 and P3. Lack of follow-up acquisitions prevented testing on further cases. Tumoral areas were outputted by identification type I for subject P2 and identification type II for subject P3, for all available follow-up examinations. The tumoral volume change is illustrated in Figure 4 where in the top subplot of each subject, SA histogram areas are shown; in the bottom subplot tumor volume change is depicted together with tumor annotation.

For the evaluation of tumor's volume change, SA histogram distributions under the two-component Gaussian mixture were extracted. Histogram area of follow-up examinations under PDF 1 were compared and assessed for volume change using Kullback-Leibler Divergence (KLD), Earth Mover's Distance (EMD) and two-sample Kolmogorov-Smirnov test (KS-test). EMD is an important perceptually meaningful metric for comparing histogram-distribution changes which measures the minimum cost required to perform a histogram matching between two histogram distributions. Therefore, it was applied as a metric to directly evaluate the distance between the entire SA and Tumor annotations through time, respectively. KS-test is a non-parametric method which uses the maximal distance between cumulative frequency distributions (CDF) in order to determine if two datasets differ significantly, and returns the

maximum difference between the CDF curves. KLD measures the distance between two density distributions and equals to zero value if and only if the two distributions are equal. Quantitative results of temporal tumor volume change of for subject P2 and P3 are shown in TABLE II. and TABLE III.

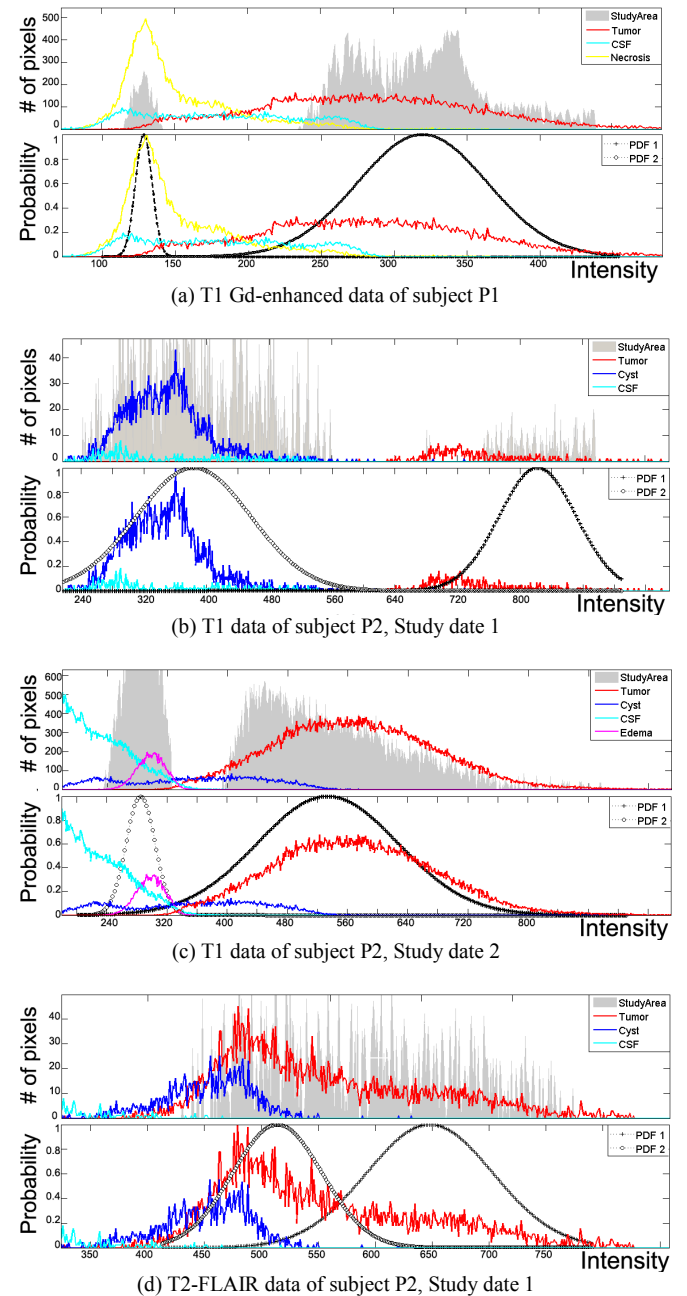


Figure 3. GMM curve fitting illustration. In top subplots SA histogram is shown in gray area; in bottom subplots the two-component GMM fits SA where tumoral area is identified by histogram data under PDF 1 (cross-dashed line) and other malignant area by data under PDF 2 (circle-dashed line). Annotations are also shown including tumor (red), CSF (cyan), necrosis (yellow), cyst (blue) and edema (magenta).

accordingly. Change percentages of specific SA histogram attributes including mean, median and standard deviation (std)

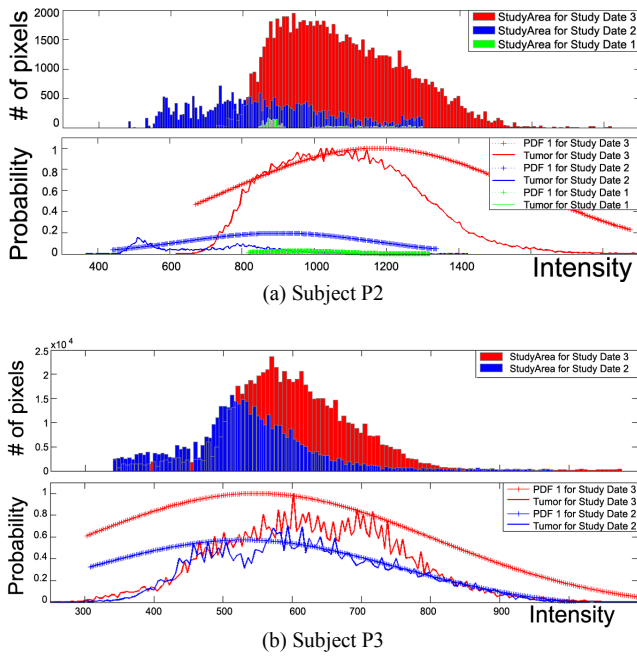


Figure 4. Tumor volume change illustration. Different colors are used to distinct study dates. In each top subplot, SA histogram areas are shown; in each bottom subplot, the corresponding GMM fit is depicted (cross-dashed line) in comparison with doctor's tumor annotation (solid line).

are presented for all follow-up examinations, together with the different distance metrics. Statistical values of SA histogram change are shown under the *PDF* column, in comparison to statistical values of tumor annotation under the *Annot* column. Cases where the percentage change was negative are depicted with a down arrow symbol ↓.

Illustrative plots showing the correspondence between SA histogram's behavior and tumor annotations are depicted in Figure 5; notice that the statistical values describing SA distributions follow the behavior of tumor annotations for the different follow-up examinations. Mean, median and std values of TABLE II. and TABLE III. are presented, together with other properties of the SA region under PDF 1 distributions, including skewness, kurtosis, interquartile range (IQR), 1st Quartile (Q1) and 3rd Quartile (Q3) values.

IV. CONCLUSION

Despite extensive opportunities to make a relatively accurate diagnosis and even if the criteria for assessing response to treatment and progressive disease have been recently revised, this process obviously has much potential for improvements. To avoid that efficacious therapy will be discontinued prematurely or that an ineffective treatment will be continued without benefit it is very important to have an accurate and standardized way of assessing the response and progress. Automated identification, quantification and volume change of tumoral and other malignant areas have been presented in current work with expected impact on the personalization of cancer treatment strategies. Further steps include integration of interpolation algorithms for constructing universal 3D volumes of same thickness, i.e. 1mm. This way,

even examinations acquired by different acquisition schemes will also be suitable for tumor volume change assessment or treatment response assessment.

Localization of malignant areas will also be considered in future steps. SA distributions provide valuable intensity information for different malignant tissues, yielding a first step towards a tissue segmentation scheme. GMM fit curves are able to characterize the intensity areas found in image slices, leading to a back-projection 3D segmentation of the malignant areas. Usually tumor consists of different kinds of pathological tissue, and can reflect independent information on different types of MRI. Multi spectra information can further be combined to enhance discrimination of abnormal tissue and enforce segmentation procedures.

TABLE II.
TUMOR VOLUME CHANGE ASSESSMENT FOR SUBJECT P2

% change of SA histogram attributes under tumoral PDF 1						
SA histogram attributes	Study Dates 1→2		Study Dates 2→3		Study Dates 1→3	
	PDF	Annot	PDF	Annot	PDF	Annot
Mean	↓ 13.48	↓ 29.03	25.42	50.83	8.52	7.04
Median	↓ 5.93	↓ 26.79	24.97	48.34	17.56	8.59
Std	29.09	96.46	↓ 8.23	11.09	18.46	118.25
# of pixels	1110	2066	177	1011	3253	23966
Volume Change Assessment						
Histogram distance metrics	Study Dates 1→2		Study Dates 2→3		Study Dates 1→3	
	PDF	Annot	PDF	Annot	PDF	Annot
KLD	0.32	0.43	0.03	0.034	0.17	0.29
EMD	133.30	294.61	217.89	366.20	88.55	111.39
K-S test	0.50	0.83	0.46	0.66	0.38	0.30

TABLE III.
TUMOR VOLUME CHANGE ASSESSMENT FOR SUBJECT P3

% change of SA histogram attributes under tumoral PDF 1			
SA histogram attributes	Study Dates 1→2		
	PDF		Annot.
Mean		11.29	1.35
Median		11.65	2.63
Std		↓ 4.45	↓ 4.00
# of pixels		54	57
Volume Change Assessment			
Histogram distance metrics	Study Dates 1→2		
	PDF		Annot.
KLD		0.0023	0.0018
EMD		61.496	14.152
K-S test		0.3163	0.0512

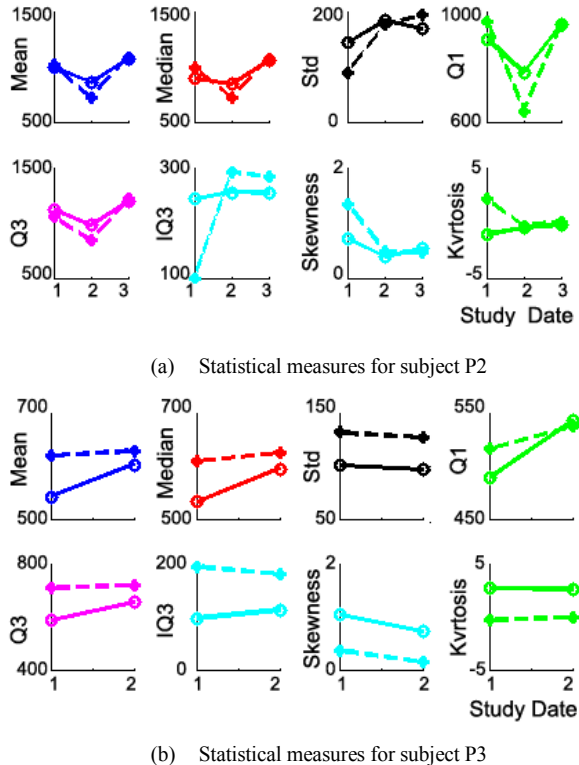


Figure 5. Graphical representation of SA histogram statistical values for subjects P2 and P3. The different study dates are depicted in the x-axis. Solid lines correspond to SA histogram under PDF 1 and dashed lines to doctor's tumor annotation.

REFERENCES

- [1] A.L. Grosu and M. Bamberg, "Gliome," *Der Onkologe*, 2011, vol 17, pp. 6-8.
- [2] D.N. Louis, H. Ohgaki, O.D. Wiestler and W.K. Cavenee, "The 2007 WHO classification of tumours of the central nervous system," *Acta Neuropathol.*, 2007, vol 114(2), pp. 97-109.
- [3] D.R. Macdonald, T.L. Cascino, S.C. Jr Schold and J.G. Cairncross, "Response criteria for phase II studies of supratentorial malignant glioma," *J Clin Oncol.*, 1990 vol. 8(7), pp. 1277-1280.
- [4] A.B. Miller, B. Hoogstraten, M. Staquet and A. Winkler, "Reporting results of cancer treatment," *Cancer* 1990, vol. 47, pp. 207-214.
- [5] World Health Organization. WHO Handbook for Reporting results of Cancer Treatment. Geneva, Switzerland: World Health Organization, 1979, pp. 14–21. (WHO offset publication; no. 48)
- [6] E.A. Eisenhauer and P. Therasse, et al, "New response evaluation criteria in solid tumours: revised RECIST guideline (version 1.1)." *Eur J Cancer*, 2009 vol. 45(2), pp. 228-247.
- [7] M. Bendszus and M. Platten, "Neuroradiological response criteria for malignant gliomas," *Nervenarzt*, 2010, vol. 81(8), pp. 950-955.
- [8] P. Sadja, "Machine Learning for Detection and Diagnosis of Disease," *Annu. Rev. Biomed. Eng.* 2006, vol. 8, pp.537-565.
- [9] N. Zhang, S. Ruan, S. Lebonvalletb, Q.M. Liao and Y.M. Zhud, "Kernel feature selection to fuse multi-spectral MRI images for brain tumor segmentation," in *CVIU*, vol. 115(2), 2011, pp. 256-269.
- [10] J. Huo, K. Okada, H.J. Kim et al., "CADrx for GBM brain tumors: predicting treatment response from changes in diffusion-weighted MRI," *Algorithms*, 2009, vol. 2, pp. 1350–1367.
- [11] A. Charnoz, V. Agnus, G. Malandain, et al., "Liver registration for the follow-up of hepatic tumors," *Medical Image Computing and Computer-Assisted Intervention*, 2005, vol. 3750, pp. 155–162.
- [12] S. Dellepiane, "Image segmentation: errors, sensitivity, and uncertainty," *Proc IEEE-Eng Med Biol Soc* 1991, vol. 13, pp. 253–254.
- [13] L.P. Clarke, R.P. Velthuizen, M.A. Camacho, et al. "MRI segmentation: methods and applications," *Magnet Reson Imaging*, 1995, vol. 13, pp. 343–368.
- [14] S.C. Zhu and A. Yuille, "Region competition: unifying snakes, region growing, and Bayes/MDL for multiband image segmentation," *IEEE Trans Patt Anal Machine Intell*, 1996, vol. 18, pp. 884–900.
- [15] M. Prastawa, E. Bullitt, N. Moon, K.V. Leemput and G. Gerig, "Automatic brain tumor segmentation by subject specific modification of atlas priors". *Acad. Radiol.* 2003, vol. 10, pp. 1341-1348.
- [16] C. Lee, M. Schmidt, A. Murtha, A. Bistriz, J. Sander, and R. Greiner, "Segmenting Brain Tumors with Conditional Random Fields and Support Vector," in *Proc. CVBIA*, 2005, vol. 3765, pp. 469–478.
- [17] J. Zhang, K. Ma, M.E. Er and V. Chong, "Tumor segmentation from magnetic resonance imaging by learning via one-class support vector machines", in *Proc. IWAIT04*, 2004; pp. 207–211.
- [18] J. Nie, Z. Xue,.; T. Liu, et al., "Wong, S.T.C. Automated brain tumor segmentation using spatial accuracy-weighted hidden Markov Random Field," *Comput. Med. Imaging Graph*, 2009, vol. 33, pp. 431–441.
- [19] J. J. Corso, E. Sharon, S. Dube, et al., "Efficient Multilevel Brain Tumor Segmentation with Integrated Bayesian Model Classification,: *IEEE Trans. Med. Imaging*, 2008, vol. 27, pp. 629-640.
- [20] J. Liu, J. Udupa, D. Odhner, D. Hackney and G. Moonis, "A system for brain tumor volume estimation via mr imaging and fuzzy connectedness," *Comput. Med. Imaging Graph*. 2005, vol. 29, pp. 21–34.
- [21] S. Dube, J.J. Corso, A. Yuille, et al., "Hierarchical Segmentation of Malignant Gliomas via Integrated Contextual Filter Response," in *Proc. SPIE*, 2008, vol. 6914, pp. 69143Y.1-69143Y.6.
- [22] S. Dube, J.J. Corso, T.F. Cloughesy, et al., "Automated MR image processing and analysis of malignant brain tumors: enabling technology for data mining," In *Data Mining Systems Analysis and Optimization in Biomedicine*; American Institute of Physics Proceedings: New York, NY, USA, 2007, vol. 953, pp. 64–84.
- [23] B. Zitova and J. Flusser, "Image registration methods: a survey", *Image and Vision Computing*, 2003, vol. 21, pp. 977–1000.
- [24] S.M. Smith, "Fast robust automated brain extraction," *Hum Brain Mapp*, 2002, vol. 17(3), pp. 143-55.
- [25] J. Zepp, N. Graf, E. Skounakis, et al., "Tumor segmentation: The impact of standardized signal intensity histograms in glioblastoma," 4th International Advanced Research Workshop on In Silico Oncology and Cancer Investigation, 2010.
- [26] M.Nixon and A. Aguado, "Feature Extraction & Image Processing", Newnes, 2002.
- [27] Y. Cointepas, J. F. Mangin, L. Garnerot, J. B. Poline, and H. Benali, "BrainVISA: Software platform for visualization and analysis of multimodality brain data," in *Proc. 7th HBM*, 2001 vol. 13, pp. S98.
- [28] L. Liang, K. Relly, R. Woods and D. Rottenberg, "Automatic segmentation of left and right cerebral hemispheres from MRI brain volumes using the graph cuts algorithm," *NeuroImage*, 2006, vol. 34 (3), pp. 1160–1170.
- [29] SurfRelax: <http://www.pc.rhul.ac.uk/staff/J.Larsson/software.html>
- [30] Y. Rubner, C. Tomasi, and L. J. Guibas, "The earth mover's distance as a metric for image retrieval," *International Journal of Computer Vision*, 2000, vol. 40, pp. 99–121.